

# Detection of Productive Oceanic Areas in the Arabian Sea and Persian Gulf Based on Reconstructed Satellite-Derived Sea Surface Temperature and Chlorophyll-a

Faisal Ahmed Khan<sup>1\*</sup>, Mengmeng Yang<sup>2</sup>, Tariq Masood Ali Khan<sup>1</sup>, Moazzam Ali Khan<sup>1</sup>

1. Institute of Environmental Studies, University of Karachi, Karachi 75270, Pakistan

2. School of Information Science and Technology, Taishan University, China

\* Corresponding Author: Email: faisal\_ahmad\_khan@hotmail.com

## Abstract

*Productive oceanic areas are rich in phytoplankton biomass, and they support a large degree of biodiversity. Therefore, it is necessary to detect productive oceanic areas to better understand their marine ecosystems. These areas are distinguished from other areas by their more frequently elevated sea surface chlorophyll-a concentrations (Chl-a) and colder sea surface temperatures (SSTs). Satellite remote sensing techniques are effective tools for ocean applications owing to their broad synoptic coverage and frequent observations. However, satellite data often include missing spatial gaps due to adverse weather conditions. In this study, monthly Moderate Resolution Imaging Spectroradiometer (MODIS)-Terra SST and Chl-a datasets were reconstructed using the Data Interpolating Empirical Orthogonal Functions (DINEOF) method to investigate their spatiotemporal variability and correlations in the Arabian Sea and the Persian Gulf (ASPG) region, which were divided into seven zones with three stations in each zone. Our results revealed that the Chl-a concentrations were much higher during the southwestern (SW) monsoon season and that the Chl-a concentration and SST exhibited a negative correlation at almost all of the stations. Furthermore, the frequency of positive Chl-a anomalies was calculated for each pixel, and the data points with frequencies of higher than 50% were regarded as productive oceanic hotspots. Maps of the average wind and Ekman transport in July were also produced and most of the hotspots were located in the upwelling regions in the ASPG, which confirms the impact of the upwelling associated with the wind in the productive oceanic areas. The results of this study provide a foundation for marine resource mapping and for effective usage of the ocean productivity in this region.*

**Keywords:** marine productivity, MODIS-Terra, data interpolation, sea surface temperature, chlorophyll-a, upwelling, Arabian sea and Persian gulf

## 1. Introduction

Productive oceanic areas are often recognized as rich areas of persistent surface chlorophyll-a (Chl-a). Fishes and other secondary consumers, such as birds and turtles, are more likely to be abundant in these areas [1]. In addition, these areas have a discrete nature in terms of their distinctive abiotic and biotic characteristics [2]. Therefore, detection of productive oceanic areas is very important for understanding a marine environment and its biodiversity.

Persistent high chlorophyll-a (Chl-a) concentrations and low sea surface temperatures (SSTs) can be used to detect productive oceanic areas [3]. Satellite-derived data have proven to be an adaptable source of information for recognizing sea surface biological dynamics, and thus, they are used as a method of predicting productive marine areas. In addition, biotic and abiotic information about sea surface water can be analyzed to explain

the primary productivity, which is prophetic for determining further biological networks linked to the surface water [1]. Ekman transport plays a vital role in regulating the oceanic biota; therefore, upwelling indices computed using wind-based calculations for each data point [4] may provide an intrinsic seasonal perspective of the oceanography of a region. Therefore, the joint investigation of satellite SST data, the Chl-a concentration, and wind data can enhance our understanding of the formation of persistent productive marine zones [5].

The utilization of satellite data, such as SST, Chl-a, and sea surface height (SSH) data, are very useful in terms of the temporal and spatial resolution. Continuous data in both space and time are desired by oceanographers to gain integrated knowledge of a marine ecosystem. However, satellite-derived data often include spatial gaps owing to adverse weather conditions, such as

clouds and rain. To overcome this problem, extensive studies have been conducted. One study, for the Arabian Sea, which mentioned the issue of cloud and its consequences for usability of oceanographic data sets [6]. Some computational techniques are very convenient in terms of increasing satellite oceanographic data [7], [8]. For example, Empirical Orthogonal Function (EOF) analysis is one of the appropriate techniques for resolving the missing data problem [9]. Empirical Orthogonal Function (EOF) analysis look for co-variability inside a data set and develops new compound variables that encapsulate that internal dependency to characterize the data's variability. The decomposition of space- and time-distributed data into modes sorted by their temporal variance is accomplished using EOF analysis, which is typically used to oceanographic and meteorological data sets [10]. Another robust method is the Data Interpolating Empirical Orthogonal Functions (DINEOF) [11], which has been widely applied to oceanographic satellite data.

The Arabian Sea and Persian Gulf (ASPG) (10–30° N, 50–75° E) (Fig. 1a) are very versatile in terms of the physical and biological fluctuations in their coastal and open sea areas. The oceanography of the ASPG is mainly based on a periodic monsoonal wind pattern. Specifically, the magnitude and direction of the wind result in the different oceanographic parameters and geographical features of the sea water having seasonal characteristics. Therefore, this region can be divided into two classes of water, i.e., coastal water and open sea water [12]. In addition, during the southwestern (SW) monsoon season, satellite data are often not available. Previous studies have investigated the basic marine biological productivity in the Arabian Sea using conventional

oceanographic methods and techniques in specific areas and seasons, but the spatial and temporal scales of these studies were limited [13]. One study focused on the impact of the monsoon on the marine productivity, and it was found that the Chl-a variations were associated with the SST fluctuations [14]. The wind patterns associated with two monsoon seasons, i.e., the southwestern monsoon (from July to September) and northeastern monsoon (from October to December), are linked to the variability of the sea surface waters [15]. Cruise-based studies have revealed that physical forcing, due to temperature and density gradients, enhanced the availability of nutrients through vertical water movement in some seasons, which mainly controlled the oceanic biota [16].

In this study, our objective was to detect the productive oceanic areas in the ASPG using the monthly Moderate Resolution Imaging Spectroradiometer (MODIS)-Terra SST and Chl-a datasets. First, we reconstructed the satellite datasets using the globally recognized DINEOF technique [7], [17], [18]. Second, the entire study area was divided into seven zones based on geographical and oceanographic features, and then, the seasonal variability of the SST and Chl-a and their relationship were investigated in each zone.

Third, the productive oceanic areas were detected based on the criteria using the per pixel Chl-a frequency [1]. However, we used a different approach to calculate the per pixel Chl-a peak counts. Then, we set a threshold value, and the pixels with values higher than the threshold were defined as persistent biologically active points.

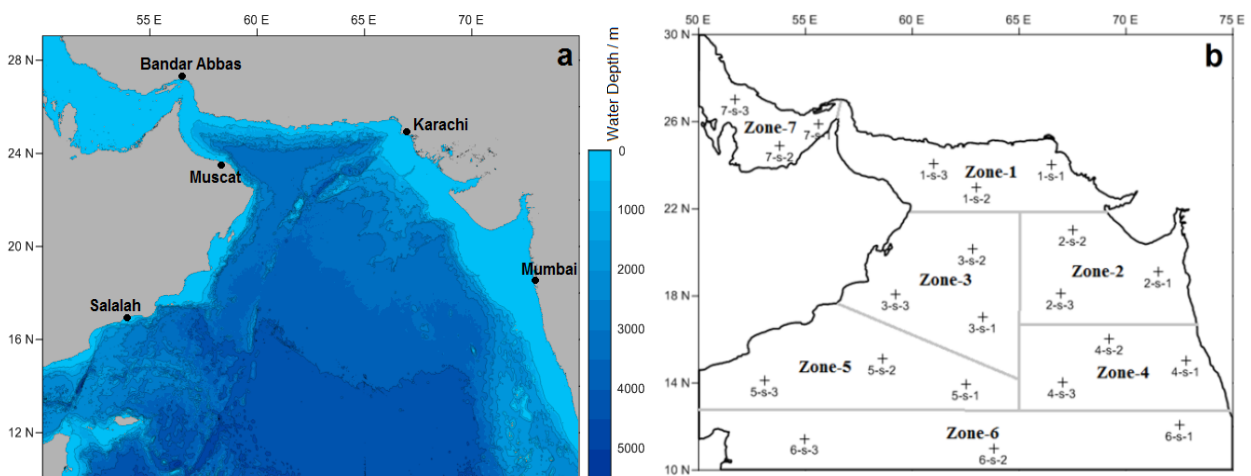


**Fig. 1:** Maps of the study area showing (a) the bathymetry of the region and (b) the locations of all of the 21 stations in the seven zones in the ASPG region

## 2. Data and Methods

### 2.1 Satellite Data and Pre-Processing

The study area was divided into seven zones (Fig. 1b), and the seasonal variabilities of the SST and Chl-a were investigated at 21 stations in these zones. To demonstrate the spatial variabilities of the SST and Chl-a, all of the stations were distributed according to the geographical significance. Zone 1 was along the Pakistan coastline, which comprises the northern boundary of the Arabian Sea. Zones 2 and 3 were located nearer to the Indian and Arabian coasts, respectively, and they included the eastern and western parts of the Arabian sea. Zone 4 was the extension of zone 2, and it consisted of the southern portion of the Indian coast. Zone 5 was along the coast of Yemen, and it extended from the coast to the open sea. Zone 6 represented the equatorial region at low latitudes. Zone 7 was the Persian Gulf region and was bounded by the major oil-producing countries of the world.

The monthly composites of the MODIS-Terra Chl-a and SST data with a 4 km spatial resolution for 2001–2017 were downloaded from the National Aeronautics and Space Administration (NASA) Ocean Biology Processing Group (<https://oceancolor.gsfc.nasa.gov/>). The data values for each station were retrieved by averaging the values from a  $3 \times 3$  matrix centered on the station. Then, the seasonal and annual SST and Chl-a were generated for each station using MATLAB, which is a useful computational tool for big datasets. In addition, the correlation statistics were calculated for the SST and Chl-a time-series for each station.

### 2.2 Climatic Data and Pre-Processing

The monthly wind data, of horizontal and vertical components which is mean of daily mean with a spatial resolution of  $0.12^\circ$  and a height of 10 m above sea level were obtained from the ERA-Interim Reanalysis datasets, which were produced by the European Centre for Medium-Range Weather Forecasting (ECMWF). The ERA-Interim Reanalysis dataset integrates quality data sources and computations for the assessment of different atmospheric variables at the global scale [19]. These monthly wind data were used to examine the seasonal variability of the wind in the ASPG region. In addition, computations (Eqs. (1) and (2)) [4] of the wind data were conducted to

obtain the Ekman transport components for each month during the study period.

$$ET_x = \frac{D_{air} c (u^2 + v^2)^{1/2} v}{D_{water} f} \quad (1)$$

$$ET_y = -\frac{D_{air} c (u^2 + v^2)^{1/2} u}{D_{water} f} \quad (2)$$

where  $u$  and  $v$  represent wind vectors from the west (positive  $u$ ) and from the south (positive  $v$ ), respectively.  $D_{air}$  is the density of air,  $D_{water}$  is the density of water,  $c$  is the drag coefficient, and  $f$  is the Coriolis parameter. The computed  $ET_x$  and  $ET_y$ , i.e., the components of the Ekman transport, were used to plot the Ekman transport for each month. The Ekman transport was used to understand the upwelling mechanism in the study area.

Upwelling regions, which account for approximately half of the worldwide fish production [20], play an important role in the estimation of the biotic dynamics of a marine region. The information extracted from the spatial distribution of these active areas can be very useful for identifying fish resources. Upwelling areas can be characterized by positive surface Chl-a anomalies and negative SST anomalies owing to the vertical movement of nutrient-rich cold seawater from the bottom layers.

### 2.3 DINEOF

Satellite data often include spatial missing gaps owing to cloud cover or rain, particularly in the monsoon seasons. Therefore, the monthly datasets were reconstructed using the DINEOF method. This technique has been proven to be a reliable statistical tool for interpolating missing data points in large datasets. The DINEOF method involves an iterative technique, which accesses the accuracy of the prediction during each repetition and selects the optimal prediction with the minimum error. Thus, it is a self-sustaining technique.

The main procedure of the DINEOF method is described below.

First, singular value decomposition (SVD) is used to calculate the EOFs as follows:

$$D = USV^T \quad (3)$$

where  $D$  is the initial matrix containing all data values with missing data points as well,  $U$  and  $V$  represent the spatial and temporal EOFs, respectively.  $S$  represents the singular values. The subscript  $T$  indicates the transpose of the array.

Second, the missing data at points  $i$  and  $j$  ( $D_{ij}$ ) are reconstructed by calculating  $k$  modes of

the EOFs using the following computational equation:

$$D_{ij} = \sum_{p=1}^{p=k} S_p (U_p)_i (V_p^T)_j \quad (4)$$

where  $U_p$  denotes the spatial EOF,  $V_p$  denotes the temporal EOF, and  $S_p$  denotes the singular value for the  $p$ th index.

Third, repeated calculations are performed for  $p$  from 1 to  $k$  to obtain the most accurate reconstructed values.

All of the monthly data were stored in a 3D matrix, with dimensions of 480 (latitude)  $\times$  600 (longitude)  $\times$  204 (time). For each matrix of monthly data, only the sea points were designated as valid data points, and the land points were excluded from the computation. Before starting the DINEOF computations, 1% of the valid data were randomly selected and were intentionally regarded as missing data. After the DINEOF reconstruction, these data were compared with the reconstructed data for cross-validation of the DINEOF method.

## 2.4 Criteria for Productive Oceanic Areas

The Chl-a concentration is a common indicator of the phytoplankton biomass [21]. Therefore, the satellite-derived Chl-a was selected as one of the indicators of productive oceanic areas. In the ASPG, the spatial distribution of the Chl-a concentration varied with the seasons throughout the year. Statistically, the data points with persistent above average Chl-a values were identified using computational techniques. Then, the peak Chl-a counts were estimated for each data point, and the data points with a greater than 50% probability of peak counts were identified.

The other two indicators were the Ekman transport calculated from the wind data and the SST. Upwelling regions often coincide with positive Chl-a anomalies and negative SST anomalies. Therefore, the combination of the surface Chl-a, SST, and wind data were used to identify the productivity hotspots. Then, these hotspots were confirmed using fishery datasets.

## 3. Results

### 3.1 DINEOF Reconstruction

The DINEOF method requires that the spatial coverage of the original satellite data is greater than 5% [11], [22]. Accordingly, 204 images were used for both the satellite SST and

Chl-a. The statistics of the DINEOF reconstruction are shown in Table 1.

One image of the original SST acquired in June 2001 and one image of the original Chl-a acquired in June 2010 were selected for comparison with the reconstructed SST and Chl-a (Figs. 2 and 3). In the original data, there were many spatial gaps, especially for Chl-a. In contrast, the reconstructed data were smooth and reasonable.

### 3.2 Validation of Reconstructed Data

The DINEOF method has a built-in cross-validation tool for validating the accuracy of the reconstructed data. In addition, we executed an independent cross-validation method. We randomly selected 1% of the valid pixels from the original satellite-derived SST and Chl-a datasets and intentionally regarded them as missing values. In addition, we retained the valid values from the original datasets and only reconstructed the data for the invalid pixels. After the DINEOF reconstruction, the reconstructed data were compared with the original data from the randomly selected dataset (Fig. 4).

For both the SST and Chl-a, the reconstructed and original data exhibited good correlations in terms of the coefficient of determination ( $R^2$ ), slope, bias, and root mean square error (RMSE). In addition, the densities of both the SST and Chl-a increased toward the 1:1 lines. Therefore, the reconstructed SST and Chl-a data were determined to be accurate and reliable.

### 3.3 Spatiotemporal Variability of Satellite SST and Chl-a

The monthly MODIS SST and Chl-a data exhibited strong seasonal variability in the ASPG region. Generally, the SST increased from the cold season (mid-November to mid-April) to the hot season (mid-April to June), decreased in the southwestern monsoon season (July to September), and then increased in the transition period (October to November). In contrast, the Chl-a decreased from the cold season to the hot season, increased in SW monsoon season, and then decreased in the transition period. In this study, February, May, August, and November were chosen as the representative months in the cold, hot, SW monsoon, and transition period, respectively (Fig. 5).

**Table 1:** Statistics of the DINEOF computations

	SST	Log <sub>10</sub> (Chl-a)
Dimensions (lat.×long.×time)	480×600×204	480×600×204
Missing data	1.75%	24.57%
Number of cross-validation points	334614	334614
Mean (input data)	27.360	-0.430
Standard deviation (input data)	1.950	0.410
Mean (output data)	27.362	-0.424
Standard deviation (output data)	1.946	0.407
Total variance explained by EOF	96%	90%
Number of optimal EOF modes	13	7

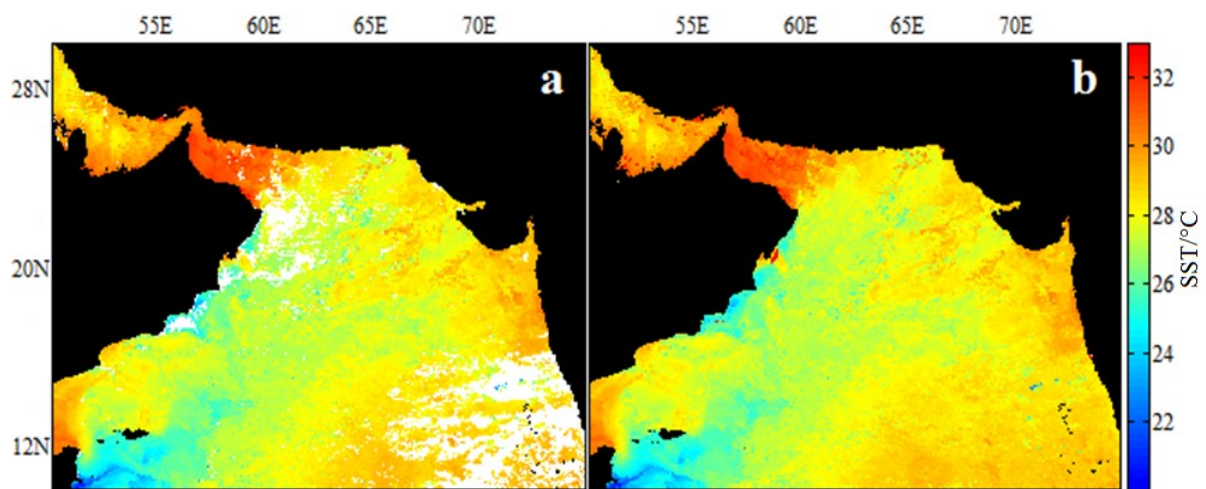


**Fig. 2:** Sea surface temperature in June 2001: (a) original cloudy data and (b) data reconstructed using the DINEOF method

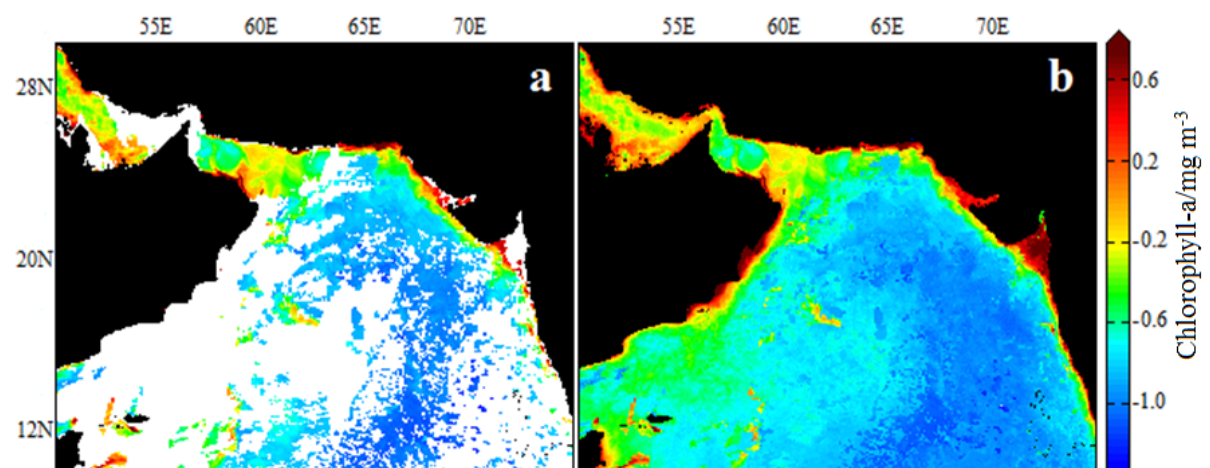


**Fig. 3:** Log<sub>10</sub> (Chl-a) in June 2010: (a) original cloudy data and (b) data reconstructed using the DINEOF method

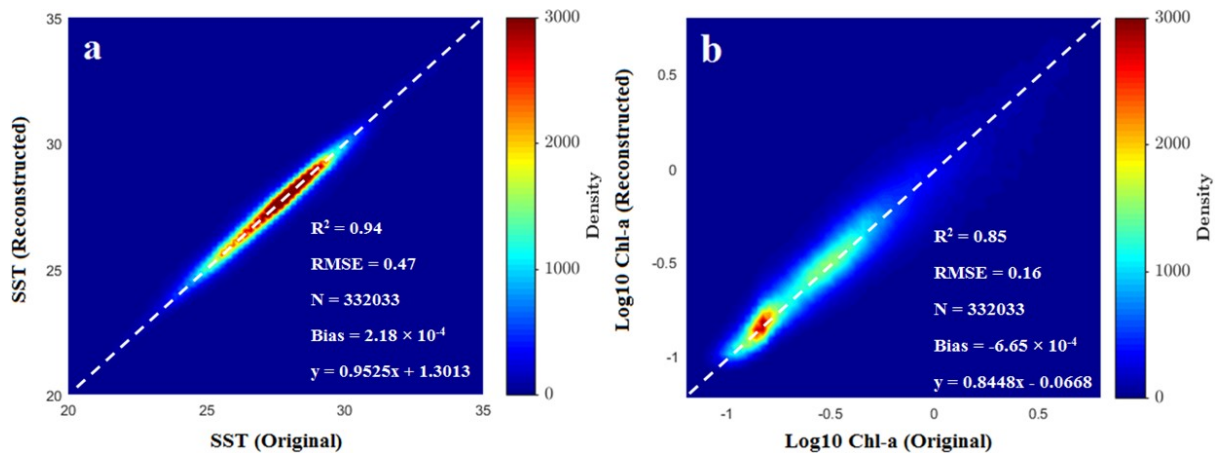


**Fig. 4:** Density plots: (a) SST (original) vs SST (reconstructed) and (b)  $\log_{10}$  Chl-a (original) vs  $\log_{10}$  Chl-a (reconstructed). The white dotted lines are the 1:1 lines

In addition, the SST and Chl-a exhibited opposite spatial variabilities in most of the ASPG region. In the cold season, the SST gradually decreased from southeast to northwest, whereas the Chl-a exhibited the opposite trend. In the hot season, the SST was almost uniformly warm in the Arabian Sea and was colder in the Persian Gulf. In contrast, the Chl-a was lower in the Arabian Sea and higher along the coasts of the Arabian Sea and the Persian Gulf. In the SW monsoon season, the SST was highest in the Persian Gulf, lowest in the southwestern part of the Arabian Sea, and gradually increased toward the southeastern part of the Arabian Sea. In contrast, the Chl-a was lower in the Persian Gulf, highest in the southwestern part, and gradually decreased toward the southeastern part of the Arabian Sea. In the transition period, the SST increased from west to southeast in the Arabian Sea, whereas the Chl-a exhibited the opposite trend.

### 3.4 Correlation between Satellite SST and Chl-a

As mentioned above, the entire study area was divided into seven zones with three stations in each zone (Fig. 1b). For each station, the SST and Chl-a time-series were investigated using all of the monthly data. In addition, the monthly data were averaged for each month, and then, the correlation between the SST and Chl-a was analyzed using the averaged data.

Based on the similarity of the correlation between the SST and Chl-a, 10 representative stations were selected in the seven zones. These stations included station 1 in zone 1 (1-s-1), station 1 in zone 2 (2-s-1), station 1 in zone 3 (3-s-1), station 1 in zone 4 (4-s-1), station 2 in zone 4 (4-s-2), station 1 in zone 5 (5-s-1), station 1 in

zone 6 (6-s-1), station 2 in zone 6 (6-s-2), station 1 in zone 7 (7-s-1), and station 2 in zone 7 (7-s-2).

For zones 1, 2, 3, and 5, all 15 stations demonstrated almost the same behavior in terms of the trends in and correlations between SST and Chl-a during the study period. Taking 1-S-1 as an example (Fig. 6a), the time-series of the monthly SST data exhibited a dominant annual cycle, except for a few anomalies in some years. The annual cycles were clearly observed, and the SST and Chl-a values exhibited two peaks almost every year. The SST exhibited one peak in summer (June) and the other in the wind transition period (October) after the SW monsoon. Chl-a exhibited the first peak in February and the second peak in September. Similarly for 2-s-1 (Fig. 6c), the SST exhibited peaks in June and October, and the Chl-a exhibited peaks in January and August. For 3-s-1 (Fig. 6e) and 5-s-1 (Fig. 6k), the maximum SST values occurred in May and October, and the maximum Chl-a values occurred in February and August. The correlation between SST and Chl-a was negative despite a lag of one month at some stations (Figs. 6b, d, f, i).

For 4-S-2 and 6-S-2, the monthly SST and Chl-a also exhibited a negative correlation. However, the maximum Chl-a values were much lower than at the stations at higher latitudes. During the study period, the Chl-a values at these two stations ranged from 0.1 to 0.5  $\text{mg m}^{-3}$ . In addition, the monthly SST and Chl-a exhibited increasing and decreasing trends, respectively, throughout the entire study period.

A direct correlation between SST and Chl-a was observed at three stations. These stations included 4-S-1 (Fig. 6g), 6-S-1 (Fig. 6m), and 7-S-2 (Fig. 6s). In contrast to 7-S-2, the SST and Chl-a

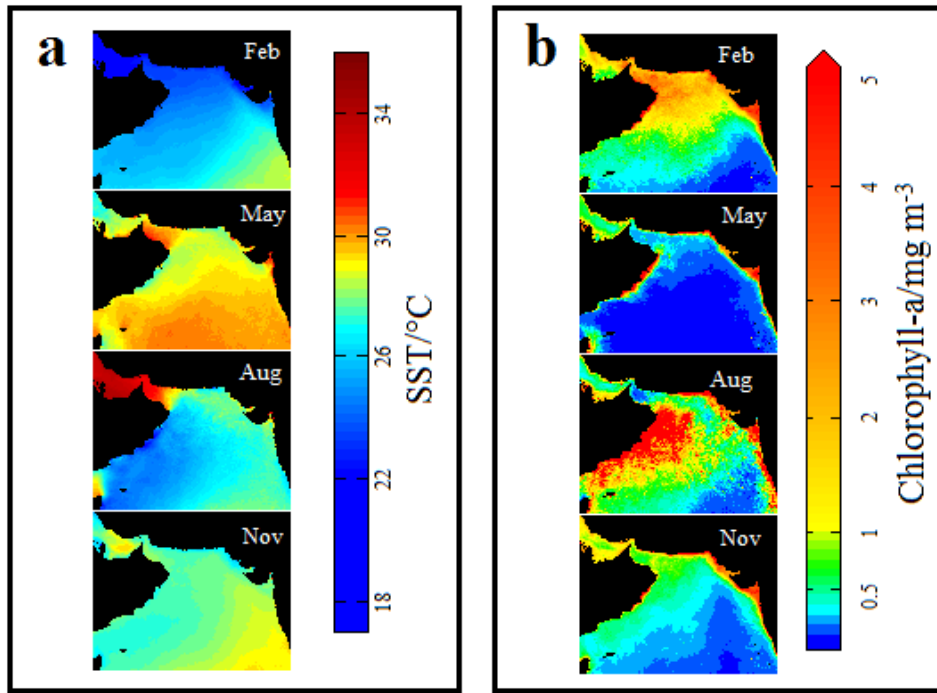
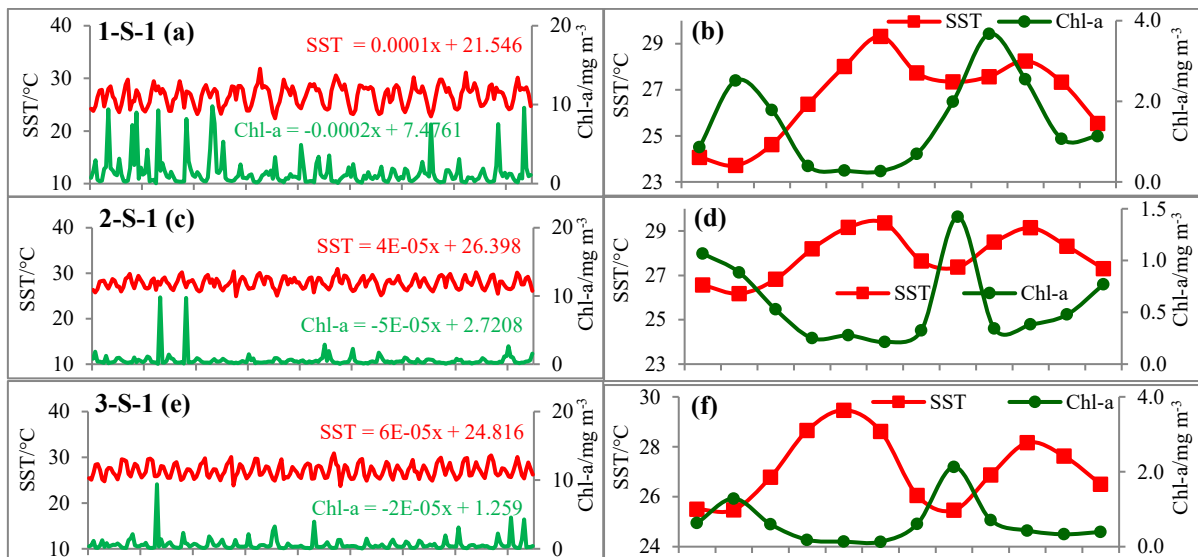


**Fig. 5:** Images of the monthly averages calculated from reconstructed MODIS data sets (a) SST and (b) Chl-a

exhibited a negative correlation at 7-S-1 (Fig. 6q). In addition, at 4-S-1, the SST and Chl-a both exhibited peaks in May and October. At 6-S-1, the SST exhibited peaks in April and October, and the Chl-a exhibited peaks in August and October. At 7-S-2, the SST and Chl-a exhibited peaks in August and September, respectively; whereas at 7-S-1, the SST exhibited a peak in July and the Chl-a exhibited a peak in February.

Considering the entire study area, the SST and Chl-a exhibited increasing and decreasing

trends, respectively, at almost all of the stations (Fig. 6). The monthly time series data for Chl-a demonstrated that the seawater was more productive during the SW monsoon seasons. In addition, for the stations nearer to the equator, the SST values were higher and exhibited fewer variations compared to the higher latitude regions throughout the year. In contrast, very low Chl-a concentrations (less than  $1 \text{ mg m}^{-3}$ ) were detected at these stations. In addition, the Chl-a and SST were negatively correlated despite the low Chl-a values.



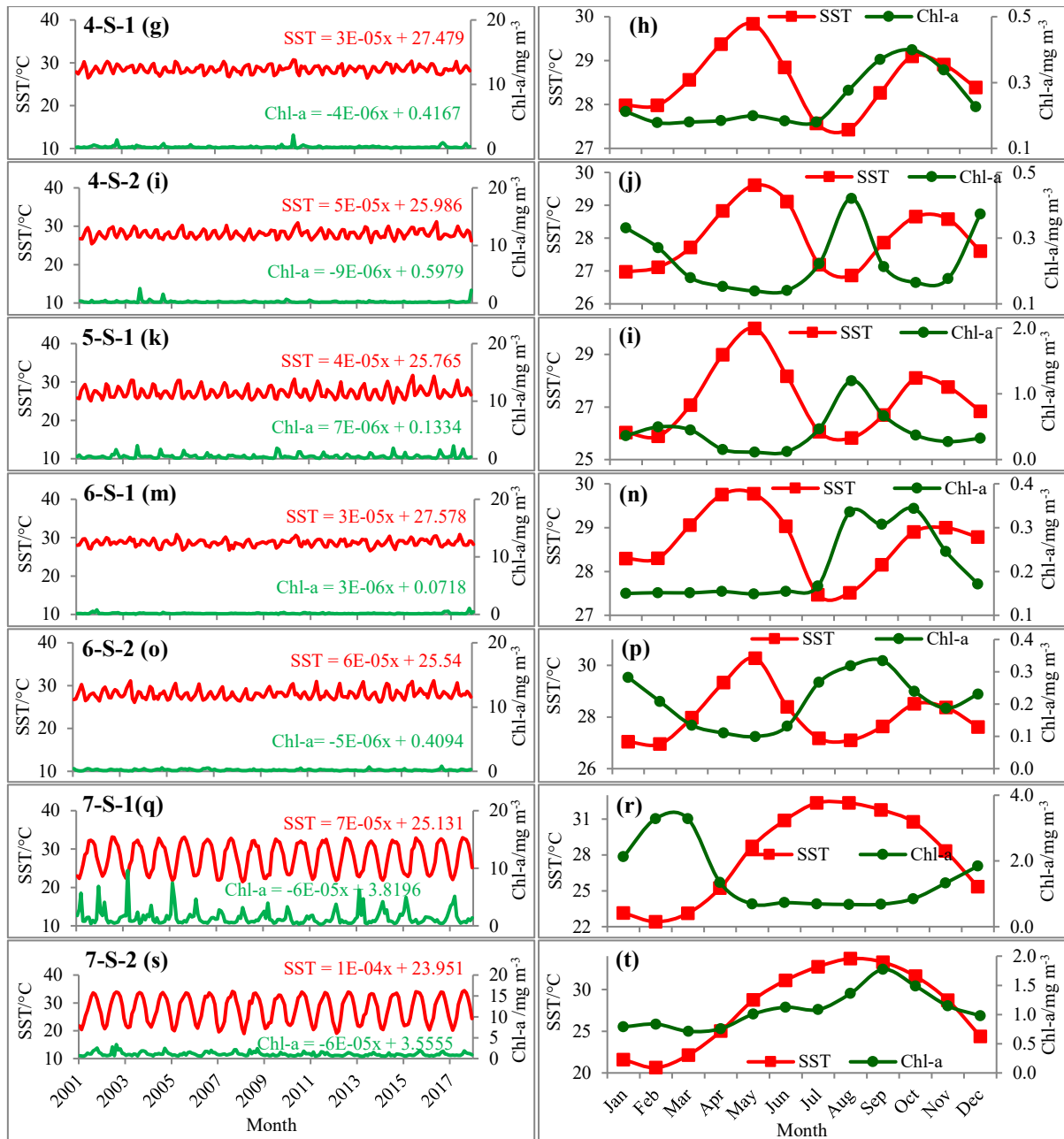


**Fig. 6:** Time-series plots of the SST and Chl-a at the selected 10 stations using (a, c, e, g, i, k, m, o, q, and s) all of the monthly data and (b, d, f, h, j, l, n, p, r, and t) the average monthly data. 1-S-1, 2-S-1, 3-S-1, 4-S-1, 4-S-2, 5-S-1, 6-S-1, 6-S-2, 7-S-1, and 7-S-2 represent station 1 in zone 1, station 1 in zone 2, station 1 in zone 3, station 1 in zone 4, station 2 in zone 4, station 1 in zone 5, station 1 in zone 6, station 2 in zone 6, station 1 in zone 7, and station 2 in zone 7, respectively

### 3.5 Distribution of Productive Oceanic Areas

The monthly Chl-a datasets were assessed to identify the persistent biologically active regions by calculating the frequencies of the positive anomalies for each pixel. The data points with frequencies of  $> 0.5$  were considered to be persistently productive. Accordingly, an image showing the positive Chl-a anomaly frequency

was produced (Fig. 7). It was estimated that 22% of the ASPG region were productive hotspots of primary productivity.

## 4. Discussion

### 4.1 DINEOF Reconstruction of MODIS SST and Chl-a in the ASPG

Oceanographic satellite datasets often

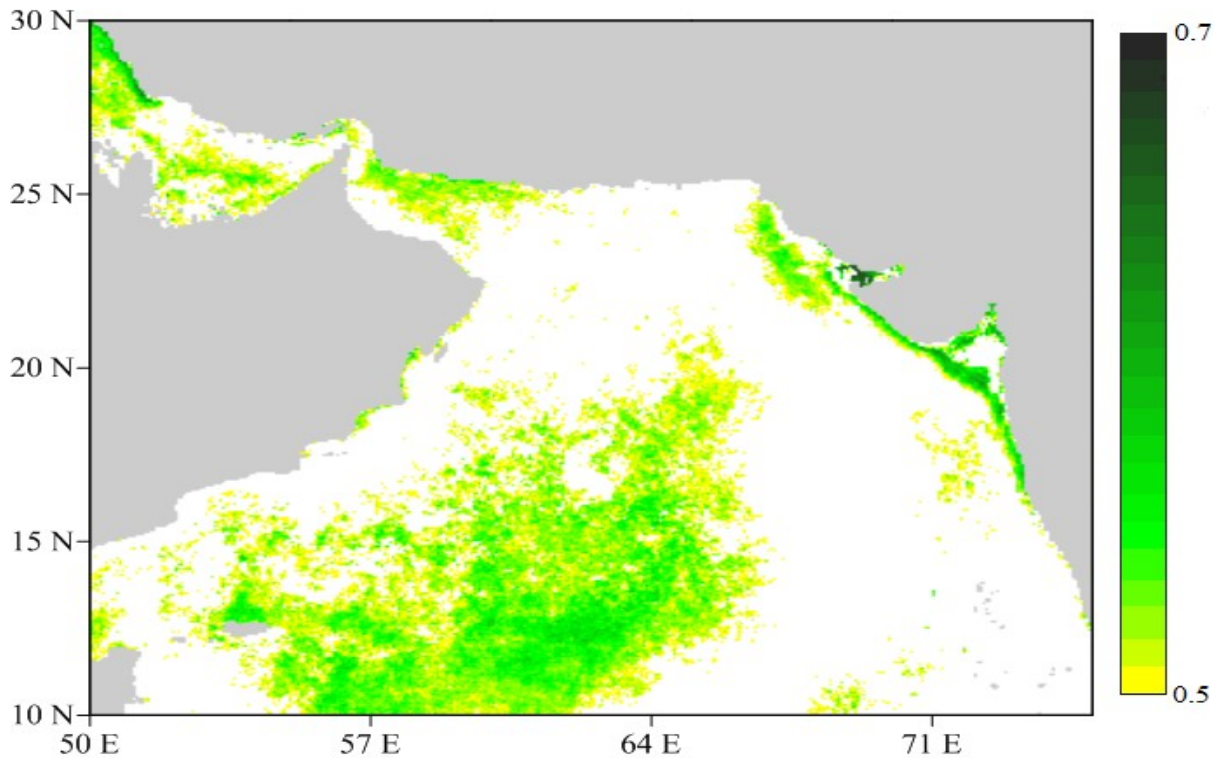


**Fig. 7:** Map of frequency of positive Chl-a anomalies (per month) in the ASPG.

include missing spatial gaps, which restricts the continuous long-term analysis of oceanic biota. In addition, this problem can result in some particular time based events going unnoticed. To overcome the issue of missing data points, the DINEOF method has been widely used, and it has been found to be reliable for interpolating oceanographic data to conduct long-term studies [23][24][7]. Reconstructed data can be utilized for the improvement of earlier studies by examining the biological productivity in unexplored seasons and regions due to missing data points [12].

Application of the DINEOF method in the ASPG under these temporal and spatial scales is exclusive to identifying marine productivity hotspots. This is because 1) continuous in-situ marine data for this region are lacking; and 2) previous studies used limited seasonal datasets with low spatial and temporal resolutions [15]. Recently, a study was conducted to reconstruct the sea surface Chl-a in the Arabian Sea using 8-day satellite data, and it was found that the DINEOF method was a reliable technique for creating a gap-free satellite dataset [25]. In this study, we focused on using monthly satellite data for the biotic and abiotic components reconstructed using the DINEOF method to identify the marine productivity hotspots in the ASPG. These hotspots

can provide a firm basis for marine resource mapping in this area [24]. In addition, the coastal communities in this region that rely on ocean resources can be provided with information about the spatial distribution of the productive regions.

The validation of the use of the DINEOF method in the ASPG revealed that the reconstructed data are accurate and reliable (Fig. 4). Accordingly, the reconstructed datasets provide a dependable consistent source of SST and Chl-a imagery for investigating the spatiotemporal variabilities of the SST and Chl-a and for identifying the productive oceanic areas.

#### **4.2 Mechanisms of the Spatiotemporal Variabilities of the SST and Chl-a**

The ASPG region is controlled by two wind patterns linked to two monsoon seasons (i.e., the SW and NE monsoon seasons). These winds highly influence the physical properties of the sea surface. This can be seen from the seasonal spatial distributions of the SST (Fig. 5). In the SW monsoon season, the wind caused the surface water to drift from the Arabian coast, which triggered upwelling and a decrease in the SST due to vertical movement of cold water from the bottom layer. The low temperature and Chl-a rich water

extended from the coast to the open sea. In contrast, in the Persian Gulf region, the stratification strengthened from summer to winter due to the lack of influence by the wind (Azizpour et al., 2014).

The sea surface chlorophyll-a distribution in the ASGP was strongly influenced by the seasonal cycle of the wind. For the entire year, the SW and NE winds, as well as the transition period in-between, defined the overall patterns of the Chl-a distribution. Upwelling brought nutrient-rich water to the surface, which enhanced the biological activity, resulting in high Chl-a concentrations, which extended from the coast to the open sea. This upwelling caused the high Chl-a concentrations in August in this region. In addition, the impacts of human interactions and freshwater discharge into the sea were also noticeable near the densely populated communities, such as the Karachi [27] and Mumbai ports [28].

In this study, results of the analysis of the correlation between the SST and Chl-a were consistent with the results of previous studies [12], and the correlation between these two variables was found to be negative in most of the study area. Because we used monthly data, the biological response in the sea surface to the variation in the SST may have lagged between two consecutive months [29]. As the results show (Fig. 6), the Chl-a peak in October lagging behind the SST peak in September at the stations where the correlation between the SST and Chl-a was negative. In zone 3, the Arabian coastlines are well-known for upwelling mechanisms all over the world, and hence, they contribute to the intense biotic activity at the western edge of the Arabian sea [30]. The summer monsoon exhibited evidence of upwelling, which transported the seawater from the lower column to the sea surface, increasing the Chl-a concentrations of the cold waters seen in the SST images (Fig. 5).

### **4.3 Detection of Productive Oceanic Areas in the ASPG**

In this study, the unit of time was one month, the frequency of persistent high Chl-a values and low SST values at all of the sea data points was computed. The consistent frequency peaks for each data point were used to identify the biologically active regions, which were considered to be ocean productivity hot spots. The MODIS data for the sea surface, which can be used to estimate the biotic resources in a wide area, were

used to estimate the biological productivity in this region.

The biotic components of a seawater environment are provided by minerals, and the spatial distributions of these minerals are highly influenced by the vertical and horizontal movements of the water masses. The seasonal variability of the distributions of these nutrients in the different water layers, from the bottom to the surface, can be determined and can be used to identify specific areas with a consistent abundance of these minerals [3]. Since the surface water is exposed to sunlight, the regions with rich nutrients are likely to be more productive, with high surface Chl-a values.

The perpetual presence of high Chl-a values indicates the productive oceanic areas in the ASPG (Fig. 7). As was previously discussed, the ASPG region is influenced by unidirectional seasonal winds. In particular, during the SW monsoon season, the consistent wind pattern causes upwelling, which enriches the surface water in nutrients and enhances the biological activity (Fig. 8). In comparison, most of the data points with a higher probability of above-average Chl-a values are located in the upwelling regions.

High Chl-a values are considered to be a proxy for large populations of phytoplankton, which serve as the foundations of all food chains in marine ecosystems [21]. Thus, the data points with persistently elevated Chl-a values are marine productivity zones. However, auspicious stations, for example, the northeastern coast and southwestern region, with biotic activeness and retention require further attention.

## **5. Conclusions**

Productive oceanic areas are characterized by low sea surface temperatures and high Chl-a concentrations. In this study, monthly MODIS-Terra SST and Chl-a datasets were precisely reconstructed using the DINEOF technique, and then, they were used to identify the productive oceanic areas in the ASPG region. The entire study area was divided into seven zones, and the seasonal variability of the Chl-a and SST and their correlation were analyzed in each zone to understand the formation of biologically active areas. Furthermore, the probability of the sea surface Chl-a concentration being above the average value was calculated for each data point, and the data points with a probability of greater than 50% were regarded as ocean productivity hotspots.

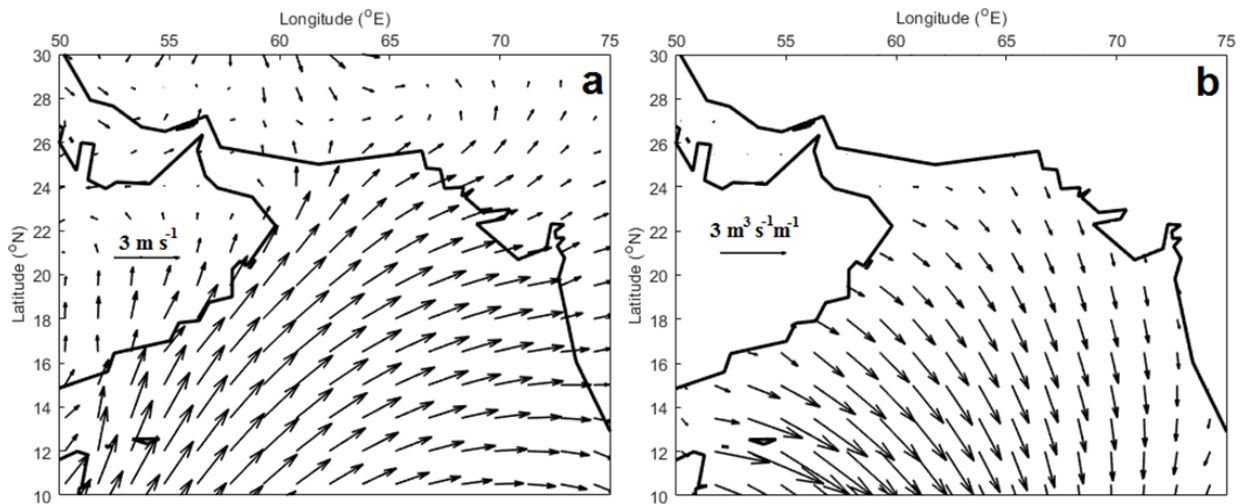


**Fig. 8:** (a) Average wind in July and (b) average Ekman transport in July.

Twenty-two percent of the data points were found to be biologically active in the ASPG region during the entire study period, and the clusters of these points were considered to be marine productivity hotspots. The most prominent sections were the southwestern region, northeastern coastal belt, and several patches in the gulf area. Regarding the temporal distribution of the productivity hotspots, the month of July contributed to the productive sea surface water due to the enhanced wind speeds. In addition, the SW monsoon season was found to be a much more productive period, with an evident upwelling mechanism associated with the speed wind in this region [31]. Although the increased SST supported the low surface Chl-a concentrations, the upwelling mechanism in the active areas led to high values in specific seasons, which is similar to the results of a previous study [5].

The results of this study provide basic insights into the biology of the surface waters in the ASPG based on a gap-free satellite-derived SST and Chl-a datasets. Based on the identified productive areas, further research can be conducted to investigate the different associated secondary food chains. In the future, fishery and/or seabird data can be utilized to enhance our understanding of the oceanography in the ASPG region.

## 6. References

- [1] R. M. Suryan, J. A. Santora, and W. J. Sydeman, "New approach for using remotely sensed chlorophyll a to identify seabird hotspots," *Mar. Ecol. Prog. Ser.*, vol. 451, pp. 213–225, 2012, doi: 10.3354/meps09597.
- [2] E. L. Hazen, R. M. Suryan, J. A. Santora, S. J. Bograd, Y. Watanuki, and R. P. Wilson, "Scales and mechanisms of marine hotspot formation," *Mar. Ecol. Prog. Ser.*, vol. 487, pp. 177–183, 2013, doi: 10.3354/meps10477.
- [3] V. D. Valavanis, A. Kapantagakis, I. Katara, and A. Pali Alexis, "Critical regions: A GIS-based model of marine productivity hotspots," *Aquat. Sci.*, vol. 66, no. 1, pp. 139–148, 2004, doi: 10.1007/s00027-003-0669-2.
- [4] P. H. Kok, M. F. M. Akhir, F. Tangang, and M. L. Husain, "Spatiotemporal trends in the southwest monsoon wind-driven upwelling in the southwestern part of the South China Sea," *PLoS One*, vol. 12, no. 2, pp. 1–22, 2017, doi: 10.1371/journal.pone.0171979.
- [5] J. P. Siemer *et al.*, "Recent Trends in SST, Chl-a, Productivity and Wind Stress in Upwelling and Open Ocean Areas in the Upper Eastern North Atlantic Subtropical Gyre," *J. Geophys. Res. Ocean.*, vol. 126, no. 8, pp. 1–20, 2021, doi: 10.1029/2021JC017268.
- [6] V. F. Banzon, R. E. Evans, H. R. Gordon, and R. M. Chomko, "SeaWiFS observations of the Arabian Sea southwest monsoon bloom for the year 2000," *Deep Sea Res. Part II Top. Stud. Oceanogr.*, vol. 51, no. 1–3, pp. 189–208, 2004.
- [7] M. Yang, F. A. Khan, H. Tian, and Q. Liu, "Analysis of the Monthly and Spring-Neap Tidal Variability of Satellite Chlorophyll-a and Total Suspended Matter in a Turbid Coastal Ocean Using the DINEOF Method," *Remote Sens.*, vol. 13, no. 4, p. 632, Feb. 2021, doi: 10.3390/rs13040632.
- [8] A. Hilborn and M. Costa, "Applications of DINEOF to satellite-derived chlorophyll-a from a productive coastal region," *Remote*

- Sens.*, vol. 10, no. 9, p. 1449, 2018.
- [9] R. E. Thomson and W. J. Emery, *Data Analysis Methods in Physical Oceanography: Third Edition*. 2014.
- [10] G. S. E. Lagerloef and R. L. Bernstein, “Empirical orthogonal function analysis of advanced very high resolution radiometer surface temperature patterns in Santa Barbara Channel,” *J. Geophys. Res. Ocean.*, vol. 93, no. C6, pp. 6863–6873, 1988.
- [11] J. M. Beckers and M. Rixen, “EOF calculations and data filling from incomplete oceanographic datasets,” *J. Atmos. Ocean. Technol.*, vol. 20, no. 12, pp. 1839–1856, 2003, doi: 10.1175/1520-0426(2003)020<1839:ECADFF>2.0.CO;2.
- [12] S. Prakash and R. Ramesh, “Is the Arabian Sea getting more productive?,” *Curr. Sci.*, vol. 92, no. 5, pp. 667–671, 2007.
- [13] S. Prasanna Kumar *et al.*, “Physical control of primary productivity on a seasonal scale in central and eastern Arabian Sea,” *Proc. Indian Acad. Sci. Earth Planet. Sci.*, vol. 109, no. 4, pp. 433–441, 2000, doi: 10.1007/bf02708331.
- [14] K. Brink *et al.*, “Monsoons boost biological productivity in Arabian Sea,” *Eos (Washington. DC)*, vol. 79, no. 13, 1998, doi: 10.1029/98eo00120.
- [15] R. T. Barber *et al.*, *Primary productivity and its regulation in the Arabian Sea during 1995*, vol. 48, no. 6–7. 2001.
- [16] J. Marra and R. T. Barber, “Primary productivity in the Arabian Sea: A synthesis of JGOFS data,” *Prog. Oceanogr.*, vol. 65, no. 2-4 SPEC. ISS., pp. 159–175, 2005, doi: 10.1016/j.pocean.2005.03.004.
- [17] X. Liu and M. Wang, “Filling the gaps of missing data in the merged VIIRS SNPP/NOAA-20 ocean color product using the DINEOF method,” *Remote Sens.*, vol. 11, no. 2, p. 178, 2019.
- [18] C. Ji, Y. Zhang, Q. Cheng, J. Y. Tsou, T. Jiang, and X. S. Liang, “Evaluating the impact of sea surface temperature (SST) on spatial distribution of chlorophyll-a concentration in the East China Sea,” *Int. J. Appl. Earth Obs. Geoinf.*, vol. 68, no. November 2017, pp. 252–261, 2018, doi: 10.1016/j.jag.2018.01.020.
- [19] D. P. Dee *et al.*, “The ERA-Interim reanalysis: Configuration and performance of the data assimilation system,” *Q. J. R. Meteorol. Soc.*, vol. 137, no. 656, pp. 553–597, 2011, doi: 10.1002/qj.828.
- [20] M. J. B. Udarbe-Walker and C. L. Villanoy, “Structure of potential upwelling areas in the Philippines,” *Deep. Res. Part I Oceanogr. Res. Pap.*, vol. 48, no. 6, pp. 1499–1518, 2001, doi: 10.1016/S0967-0637(00)00100-X.
- [21] Y. Huot and M. Babin, “Does chlorophyll &i&gt;a&lt;i&gt; provide the best index of phytoplankton biomass for primary productivity studies?,” *Does chlorophyll a Provid. best index Phytoplankt. biomass Prim. Product. Stud.*, vol. 4, no. 2, pp. 707–745, 2007, doi: 10.5194/bgd-4-707-2007.
- [22] A. Alvera-Azcárate, A. Barth, M. Rixen, and J. M. Beckers, “Reconstruction of incomplete oceanographic data sets using empirical orthogonal functions: Application to the Adriatic Sea surface temperature,” *Ocean Model.*, vol. 9, no. 4, pp. 325–346, 2005, doi: 10.1016/j.ocemod.2004.08.001.
- [23] C. Ji, Y. Zhang, Q. Cheng, J. Y. Tsou, T. Jiang, and X. S. Liang, “Evaluating the impact of sea surface temperature (SST) on spatial distribution of chlorophyll-a concentration in the East China Sea,” *Int. J. Appl. Earth Obs. Geoinf.*, vol. 68, no. January, pp. 252–261, 2018, doi: 10.1016/j.jag.2018.01.020.
- [24] A. Hilborn and M. Costa, “Applications of DINEOF to satellite-derived chlorophyll-a from a productive coastal region,” *Remote Sens.*, vol. 10, no. 9, pp. 11–13, 2018, doi: 10.3390/rs10091449.
- [25] C. Jayaram, N. Priyadarshi, J. Pavan Kumar, T. V. S. Udaya Bhaskar, D. Raju, and A. J. Kochuparampil, “Analysis of gap-free chlorophyll-a data from MODIS in Arabian Sea, reconstructed using DINEOF,” *Int. J. Remote Sens.*, vol. 39, no. 21, pp. 7506–7522, 2018, doi: 10.1080/01431161.2018.1471540.
- [26] J. C. Azizpour Vahid; Khosravi, Maziar; Einali, Abbas Irani, “Study of the Physical Oceanographic Properties of the Persian Gulf, Strait of Hormuz and Gulf of Oman Based on PG-GOOS CTD Measurements,” *Mar. Pollut. Bull.*, vol. 5, no. 18, pp. 35–59, 2014.
- [27] Y. Nergis, M. Sharif, A. F. Choudhry, A. Hussain, and J. A. Butt, “Impact of industrial and sewage effluents on Karachi coastal water and sediment quality,” *Middle-East J. Sci. Res.*, vol. 11, no. 10, pp. 1443–1454, 2012.
- [28] T. Balasubramanian, “Heavy metal contamination and risk assessment in the marine environment of Arabian Sea, along the southwest coast of India,” *Am. J. Chem.*, vol. 2, no. 4, pp. 191–208, 2012.
- [29] D. R. Barlow, H. Klinck, D. Ponirakis, C. Garvey, and L. G. Torres, “Temporal and spatial lags between wind, coastal upwelling,

- and blue whale occurrence,” *Sci. Rep.*, vol. 11, no. 1, pp. 1–10, 2021, doi: 10.1038/s41598-021-86403-y.
- [30] V. Praveen, R. S. Ajayamohan, V. Valsala, and S. Sandeep, “Intensification of upwelling along Oman coast,” no. May, 2016, doi: 10.1002/2016GL069638.1.
- [31] L. M. Beal, V. Hormann, R. Lumpkin, and G. R. Foltz, “The response of the surface circulation of the arabian sea to monsoonal forcing,” *J. Phys. Oceanogr.*, vol. 43, no. 9, pp. 2008–2022, 2013, doi: 10.1175/JPO-D-13-033.1.